Carbon 122 (2017) 106–113

Contents lists available at ScienceDirect

Carbon

journal homepage: www.elsevier.com/locate/carbon

Graphene-supported highly crosslinked organosulfur nanoparticles as cathode materials for high-rate, long-life lithium-sulfur battery

Shuaibo Zeng [a], Ligui Li [a, b, *], Lihong Xie [a], Dengke Zhao [a], Ni Zhou [a], Nan Wang [a], Shaowei Chen [a, c, **]

[a] Guangzhou Key Laboratory for Surface Chemistry of Energy Materials, New Energy Research Institute, College of Environment and Energy, South China University of Technology, Guangzhou Higher Education Mega Center, Guangzhou 510006, China
[b] Guangdong Provincial Key Laboratory of Atmospheric Environment and Pollution Control, College of Environment and Energy, South China University of Technology, Guangzhou 510006, China
[c] Department of Chemistry and Biochemistry, University of California, 1156 High Street, Santa Cruz, CA 95064, USA

ARTICLE INFO

Article history:
Received 31 March 2017
Received in revised form
4 June 2017
Accepted 14 June 2017
Available online 18 June 2017

Keywords:
Lithium-sulfur battery
Rate performance
Cycling stability
Sulfur copolymer

ABSTRACT

Lithium-sulfur batteries represent one of the next-generation Li-ion batteries; yet rapid performance degradation is a major challenge. Herein, a highly crosslinked copolymer is synthesized through thermally activated polymerization of sulfur and trithiocyanuric acid onto the surface of reduced graphene oxide nanosheets. Of the thus-synthesized composites, the sample with a high sulfur content of 81.79 wt.% shows a remarkable rate performance of 1341 mAh g^{-1} at 0.1 C and 861 mAh g^{-1} at 1 C with an almost 100% coulombic efficiency. The composite electrode also effectively impedes the dissolution of polysulfides and their shuttle diffusion because of the abundant and robust chemical bonding between sulfur and trithiocyanuric acid and spatial confinement of polysulfides by the reduced graphene oxide sheets, which leads to 81.72% retention of the initial capacity even after 500 deep charge-discharge cycles at 1 C, corresponding to a decay rate of only 0.0404% per cycle. This performance is markedly better than those of comparative materials prepared in a similar fashion but at either higher or lower S loading, and among the highest in sulfur copolymer cathodes to date. The results provide an effective paradigm in the preparation and engineering of polymer cathode materials for high-performance lithium-sulfur batteries.

1. Introduction

Lithium-sulfur (Li-S) batteries are regarded as one of the most promising candidates for next-generation rechargeable batteries due to various unique advantages: (a) the energy density of Li-S batteries (2567 Wh Kg^{-1}) is about five times higher than that of conventional Li-ion batteries due to the high specific capacity of sulfur (1672 mAh g^{-1}), such that Li-S batteries can meet the ever-increasing power demands in portable electronics and electric vehicles [1–3]; (b) sulfur is among the most earth-abundant elements and may sustain massive commercialization of Li-S batteries [4,5]; and (c) Li-S batteries are easy to fabricate, cost-effective and environmentally friendly [6–8]. However, to realize large-scale commercialization of Li-S batteries, several critical issues need to be resolved, such as the low coulombic efficiency and rate capacity resulting from the low electrical conductivity of sulfur and polysulfides (~5×10^{-30} S cm^{-1} at 25 °C) [9,10], rapid capacity attenuation caused by mechanical degradation of the cathode due to the large volume expansion (up to 80%) of sulfur lithiation, and the so-called "shuttle" effect of lithium polysulfides (Li_2S_n with $4 \leq n \leq 8$) due to the dissolution and diffusion of polysulfides in organic electrolytes [11–14]. Moreover, lithium dendrites can be easily formed in the lithium metal anode during charge-discharge processes, which may short the circuit by penetration into the thin membrane, resulting in a short life-span and serious safety concerns [15].

To mitigate these issues, extensive research efforts have been devoted to the design and engineering of novel cathode materials

* Corresponding author. Guangzhou Key Laboratory for Surface Chemistry of Energy Materials, New Energy Research Institute, College of Environment and Energy, South China University of Technology, Guangzhou Higher Education Mega Center, Guangzhou 510006, China.
** Corresponding author. Department of Chemistry and Biochemistry, University of California, 1156 High Street, Santa Cruz, CA 95064, USA.
E-mail addresses: esguili@scut.edu.cn (L. Li), shaowei@ucsc.edu (S. Chen).

http://dx.doi.org/10.1016/j.carbon.2017.06.036
0008-6223/

[16,17], membrane separators [18–20], and anode protections [21] to prevent the dissolution and diffusion of polysulfides in the electrolyte and the formation of lithium dendrites [22–24]. As for cathode materials, a variety of carbon-based materials, such as hollow carbon spheres [25–27], carbon nanotubes [20,28,29], porous carbon [3,30–32], layered carbon matrices [33], and carbon nanofibers [34,35], have been widely used as conductive substrates for sulfur to increase the rate performance and coulombic efficiency. However, sulfur is mostly physically adsorbed on these carbon substrates, hence the issues of dissolution and diffusion of polysulfides in organic electrolytes remain unresolved [36–38]. This may be further mitigated by chemical confinement of the carbon-sulfur composites. An emerging judicious method is based on copolymerization of elemental sulfur with small organic molecules such as vinylic monomers [4], styrene [39], polyacrylonitrile [40] and dicyanobenzene [41] through inverse vulcanization. However, the insulating nature of these copolymers greatly restricts the loading of active sulfur to only 1 mg cm^{-2} or lower (shown in Table S1) and hence compromises the capacitive performance. Therefore, deliberate engineering of the sulfur copolymer-based cathodes is strongly desired to increase the loading of active sulfur for further improvement of the battery performance. This is the primary motivation of the present work.

Herein, we report the preparation of graphene-supported highly crosslinked sulfur copolymer nanoparticles as a cathode material for Li-S battery. Experimentally, trithiocyanuric acid (TTCA) was pre-deposited on the surface of highly conductive graphene oxide nanosheets as tiny nanoparticles, and then crosslinked with sulfur via radical polymerization. The resulting cp(S-TTCA)@rGO hybrids exhibited much enhanced electrical conductivity, as compared to the nanocomposites without graphene support, and the dissolution and diffusion of polysulfides was effectively supressed by the combined contributions of chemical confinement resulting from the extensive bonding between sulfur and TTCA as well as physical confinement by the graphene crosslinked networks. Within the present experimental context, the sample with a high sulfur content of 81.79 wt.% (2.0 mg cm^{-2}) was found to exhibit the best performance as the cathode for Li-S battery, with a reversible capacity of 1341 mAh g^{-1} at 0.1 C, and a discharge capacity of 671 mAh g^{-1} even after 500 deep charge-discharge cycles at 1 C with a high capacity-retention of 81.72%.

2. Experimental section

2.1. Synthesis of cp(S-TTCA)@rGO nanocomposites

Graphene oxide was obtained by a modified Hummers' method [42]. As illustrated in Fig. 1, *cp(S-TTCA)@rGO* was synthesized as follows: (1) TTCA was dissolved in dimethyl formamide (DMF, 99%, Alfa Aesar) to form a solution (1.13 M), followed by the addition of graphene oxide (50 mL, 8 g L^{-1}). After magnetic stirring of the mixed solution for 2 h, a calculated amount of sodium borohydride was slowly added to the solution also under magnetic stirring for another 2 h. The obtained TTCA@rGO composites were collected by filtering, washed with distilled water and then dried. (2) The obtained TTCA@rGO was mixed with sulfur at a TTCA@rGO:sulfur weight ratio of 2:4, 1:4 and 1:7; and the mixtures were heated at 150 °C for 3 h to impregnate the molten sulfur into the pores between rGO sheets under an argon atmosphere, and then further heated at 170 °C for 8 h to initiate ring-opening polymerization of sulfur and TTCA, leading to the formation of highly crosslinked nanoparticles between S and TTCA that were supported on rGO nanosheets. The resulting composites were denoted as cp(S-TTCA)@rGO-70, cp(S-TTCA)-80 and cp(S-TTCA)-90, respectively. Simple cp(S-TTCA) was also prepared in a similar fashion but without the addition of graphene or carbon black.

The cp(S-TTCA)@rGO-80/C composite was prepared with a mixture of cp(S-TTCA)@rGO-80, carbon black and PVDF at a mass ratio of 80: 10: 10.

2.2. Material characterization

SEM and TEM measurements were conducted on a Hitachi S-4800 field emission scanning electron microscope (FESEM) and a JEOL JEM-2100 transmission electron microscope at an acceleration voltage of 200 KV, respectively. X-ray diffraction (XRD) measurements were performed with a Bruker D8 instrument using Cu K_α radiation. FTIR spectra were recorded on Nicolet 6700 FTIR spectrometer using a KBr pellet in the transmission mode. Raman spectra were recorded on a RENISHAW in Via instrument with an Ar laser source of 488 nm in a macroscopic configuration. XPS measurements were carried out with a Phi X-tool XPS instrument. TGA/DSC curves were acquired with a METTLER instrument under a N_2 atmosphere at a heating rate of 10 °C min^{-1}.

2.3. Device preparation and characterization

In a typical measurement, the polyvinylidene fluoride (PVDF) binder was completely dissolved in *N*-methyl-2-pyrrolidene (NMP) under magnetic stirring. A calculated amount of the cp(S-TTCA)@rGO samples prepared above and conductive carbon black were then added into the solution to form a homogenous slurry at a cp(S-TTCA)@rGO: carbon black: PVDF mass ratio of 80: 10: 10. The slurry was then deposited on an aluminium current collector using the doctor blade method and then dried at 60 °C for 18 h in a vacuum oven. The obtained cathode foil was compressed and cut into circular sheets of 12 mm in diameter. The typical mass loading of active sulfur was calculated to be 2.0 mg cm^{-2}. The CR2032-type experiment cells were assembled in an argon-filled glove box. The cell comprised of a positive electrode, polypropylene (PP diaphragm Celgard 2400) as the separator, a lithium foil as the reference/counter electrode, and the mixed solution of 1,3-dioxolane and 1,2-dimethoxyethane (volume ratio 1:1) containing 1 M lithium bis(trifluoromethanesulfonyl) imide (LiTFSI), and 0.1 M $LiNO_3$ as the electrolyte. For comparison, coin-cells with cp(S-TTCA) and S cathodes were prepared in the same manner, at the same active substance content and mass loading of active sulfur.

Galvanostatic discharge-charge tests of the as-fabricated cells were performed by potential cycling between +1.5 and + 3.0 V (vs. Li/Li^+) at different current rates using a button cell test system (LANHE CT2001A 5 V 20 mA). Cyclic voltammetry (CV) studies were performed in the potential range of +1.5 to +3.0 V at varied scan rates. EIS studies were conducted at the charged state in the frequency range of 100 KHz to 10 mHz at an AC amplitude of 5 mV.

3. Results and discussion

The synthesis of cp(S-TTCA)@rGO was illustrated in Fig. 1, where TTCA and graphene oxide (GO) nanosheets were firstly co-dissolved in *N*,*N*-dimethyl formamide, followed by the addition of an aqueous solution of $NaBH_4$ that produced reduced GO (rGO) and concurrently precipitated and deposited crystalline TTCA nanoparticles onto the rGO surface to form TTCA@rGO composites (shown in Fig. S1). The mixture of sulfur and TTCA@rGO was then heated at 170 °C where ring-opening radical polymerization of sulfur and TTCA yielded cp(S-TTCA)@rGO as the final product. The formation of crosslinked cp(S-TTCA) was evidenced by the color change from light yellow (TTCA) to dark-brown (shown in Fig. S2) [43].

Three samples were prepared at various S loadings.

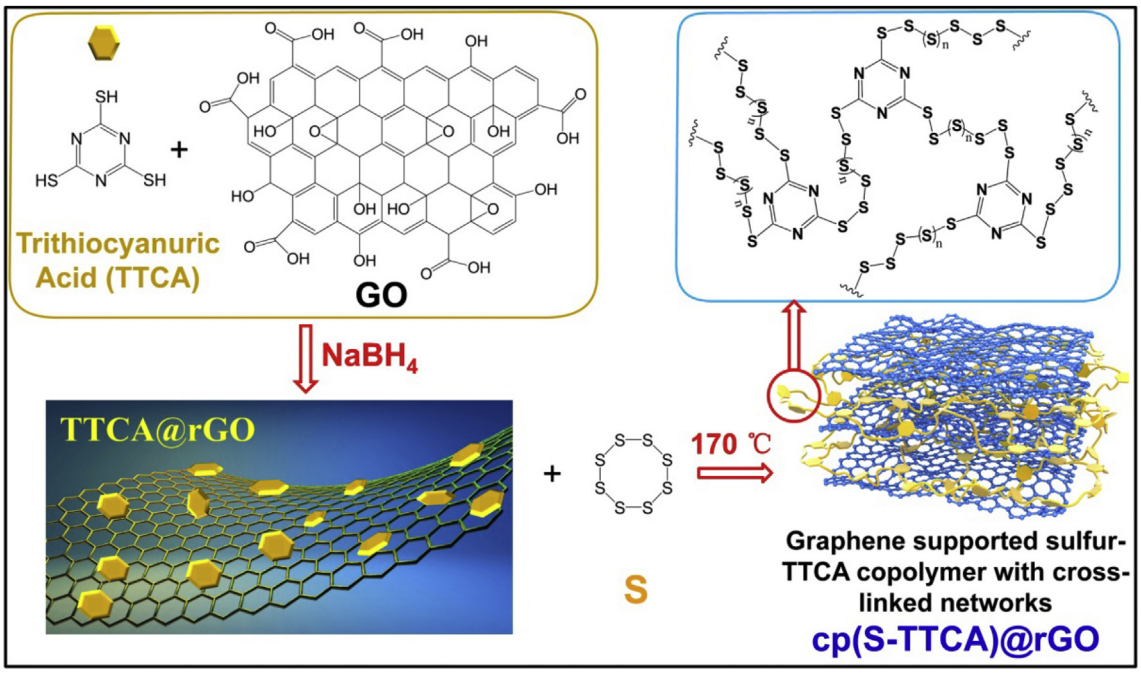

Fig. 1. Schematic illustration of the synthesis of graphene-supported crosslinked sulfur copolymer nanoparticles, cp(S-TTCA)@rGO. (A colour version of this figure can be viewed online.)

Thermogravimetric analysis (TGA) was then carried out in a nitrogen atmosphere to determine the sulfur content [15,44,45]. From Fig. 2a, one can find that all three samples exhibited a major weight loss that started at ca. 200 °C and ended at ca. 350 °C,

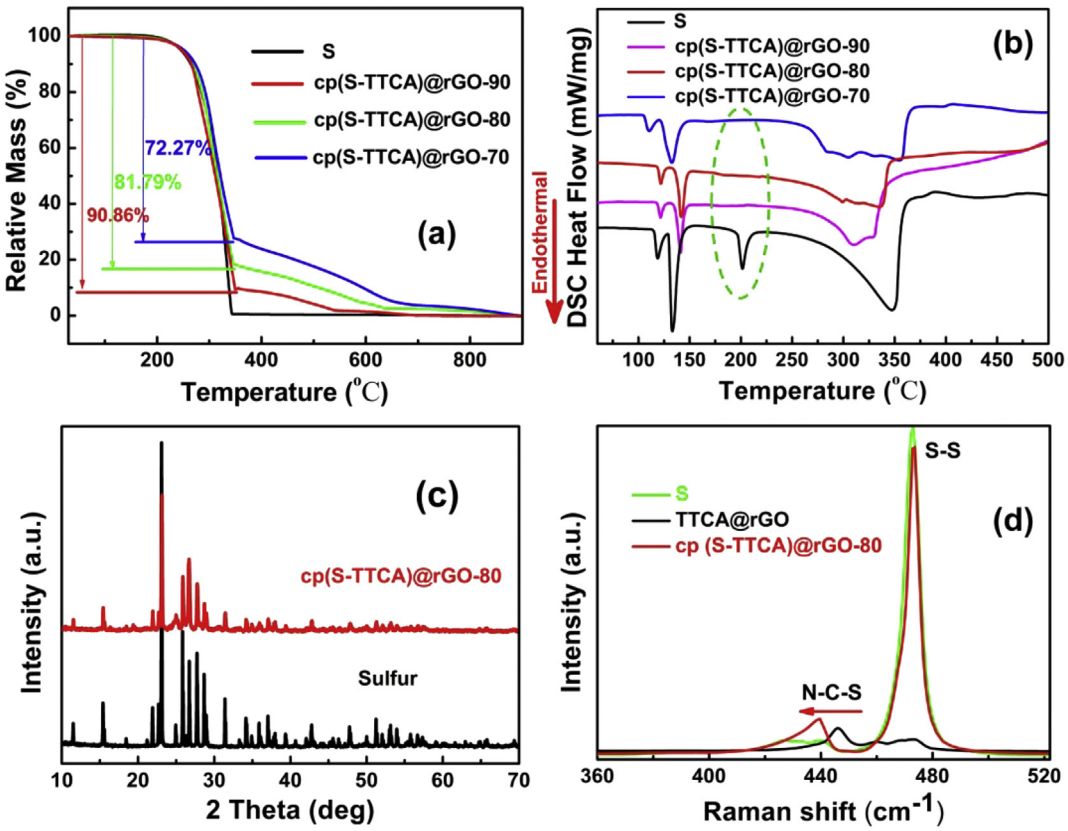

Fig. 2. (a, b) TGA and DSC curves of elemental S and cp(S-TTCA)@rGO with different sulfur contents. (c) XRD patterns of elemental S and cp(S-TTCA)@rGO-80. (d) Raman spectra of elemental S, TTCA@rGO and cp(S-TTCA)@rGO-80. (A colour version of this figure can be viewed online.)

consistent with that of elemental sulfur. This suggests that such a weight loss was due to the evaporation of sulfur nanocrystals in the nanocomposites [46]. From the weight loss, the sulfur contents were estimated to be 72.27 wt.%, 81.79 wt.%, and 90.86 wt.%. Thus, the three samples were referred to as cp(S-TTCA)@rGO-70, cp(S-TTCA)@rGO-80, and cp(S-TTCA)@rGO-90, respectively. DSC measurements were conducted to further ascertain the formation of crosslinking between sulfur and TTCA. As shown in Fig. 2b, pure sulfur sample exhibited four pronounced endothermic peaks in the heating thermogram, where the first one at ca. 118 °C was ascribed to the solid phase transformation from orthorhombic to monoclinic forms, the second one at ca. 134 °C was attributed to the transformation from solid to liquid state (melting), and the third one at about 200 °C was due to the ring-opening of S_8 to form radicals; whereas, the fourth peak centered at ca. 350 °C was marked broad, starting from ca. 250 °C to about 360 °C, which is probably due to the combination of evaporation and boiling of liquid sulfur, coinciding with the sudden weight loss within this temperature range in the corresponding TGA curve for pure sulfur in Fig. 2a. For the three cp(S-TTCA)@rGO composites, the endothermic peaks at ca. 110 °C, 134 °C and 350 °C were also well-resolved, whereas the peak at about 200 °C completely disappeared, as highlighted by a green ellipse in Fig. 2b. This observation signifies that S_8 ring has been opened to bond/anchor with thiol groups on TTCA, that is formation of crosslinked polymers in these three cp(S-TTCA)@rGO composites. Note that the significant weight loss of TTCA is also at about 330 °C due to decomposition (Fig. S3), therefore the weight loss and endothermal peak at around this temperature for the three cp(S-TTCA)@rGO composites depicted in Fig. 2b should be partially contributed by the decomposition of TTCA.

From Fig. 2c, one can see that the XRD patterns of cp(S-TTCA)@rGO-80 resembled those of elemental sulfur, which indicates that sulfur remained crystalline in the composite. The bonding interaction between elemental sulfur and TTCA was evidenced in Raman measurements. Fig. 2d shows the typical Raman spectra of S, TTCA@rGO and cp(S-TTCA)@rGO-80. For TTCA@rGO, the vibrational band at ca. 446 cm^{-1} might be attributed to the N=C–S deformation in TTCA [43]. After the mixture of TTCA and elemental sulfur was heated at 170 °C to produce cp(S-TTCA)@rGO-80, this deformation peak red-shifted to 439 cm^{-1} and concurrently a new peak appeared at ca. 473 cm^{-1} due to the stretching of the S–S bonds. Again, these observations suggest that elemental sulfur (S_8) reacted with the thiol groups on TTCA forming crosslinked polymers, as depicted in Fig. 1.

The morphology of the cp(S-TTCA)@rGO composites was then studied by scanning electron microscopy (SEM) measurements. As depicted in Fig. 3a, granular domains with diameters ranging from tens of nanometers to hundreds of nanometers are observed with pure sulfur, whereas cp(S-TTCA)@rGO-80 exhibited a sheet-like crumpled structure with a rough surface (shown in Fig. 3b). From higher-magnification SEM studies of the selected area in Fig. 3b, one can see that nanoparticles up to 50 nm in width are densely packed on these sheet-like structures (shown in Fig. 3c). Typical TEM images of the cp(S-TTCA)@rGO-80 are shown in Fig. 3d and e, where one can find that the nanoparticles in Fig. 3c are actually comprised of smaller particles of less than 20 nm in diameter. In the corresponding high-resolution TEM image shown in Fig. 3f, one can see well-resolved lattice fringes with a d-spacing of 0.38 nm, consistent with the (222) planes of crystalline sulfur (PDF#08-0247) [47], indicating the encapsulation of nanocrystalline sulfur in the cp(S-TTCA)@rGO composites. EDS measurements (shown in Fig. 3g) show that the cp(S-TTCA)@rGO-80 composite was comprised only of the C, O, N, and S elements, which were distributed homogeneously on the surface of the sample, as evidenced in elemental mapping studies (shown in Fig. 3i). Calculations based on the integrated peak areas yielded a content of 15.45 wt.% for C, 1.02 wt.% for O, 4.67 wt.% for N and 78.85 wt.% for sulfur (shown in Fig. 3h). Consistent results were obtained in XPS measurements, where the contents of C, N and S were determined to be 18 wt.%, 7 wt.% and 75 wt.%, respectively (shown in Fig. S4).

The performance of the cp(S-TTCA)@rGO composites as active cathode materials was then evaluated with a prototype battery in a coin-cell configuration, as depicted in Fig. 4a and Fig. S5. In cyclic voltammetric (CV) measurements (shown in Fig. 4b), two pronounced reduction peaks were resolved in the negative potential scan from +3.0 V to +1.5 V for the cp(S-TTCA)@rGO-80 cathode, where the first peak at about +2.23 V was attributed to the conversion of polymerized sulfur in cp(S-TTCA) to high-ordered polysulfides (Li_2S_n, $4 \leq n \leq 8$) while the second peak at about +1.93 V was ascribed to the further reduction of lithium polysulfides to lithium sulfides (Li_2S). In the charging state, an anodic peak emerged at about +2.51 V, which arose from the oxidation of Li_2S to polysulfides [48]. It is worthy to note that no obvious change was observed between the 1st and 20th CV cycles of cp(S-TTCA)@rGO-80, which signifies high electrochemical stability of the cp(S-TTCA)@rGO-80 cathode. To identify the effect of sulfur-rich nanoparticles on the electrical performance of cp(S-TTCA)@rGO-80, electrochemical impedance spectroscopic (EIS) measurements was then conducted. From the EIS spectra in Fig. 4c, one can see that both the cp(S-TTCA)@rGO-80 sample and a simple mixture of sulfur and carbon black (S/C) showed a semicircle in the high-frequency region and a radial oblique line in the low-frequency region. From the semicircles, the electron-transfer resistance (R_{ct}) involved was estimated to be only 51.2 Ω for the cp(S-TTCA)@rGO-80 cathode, markedly lower than that (132.9 Ω) of the S/C electrode [49]. As for the linear segment in the low-frequency region, it was ascribed to the resistance of ion diffusion within the electrodes. Again the cp(S-TTCA)@rGO-80 showed a much lower resistance than the S/C electrode. These observations clearly demonstrate that copolymerization of sulphur with TTCA to form crosslinked nanoparticles on rGO significantly facilitated the electron-transfer and mass-transfer dynamics.

Notably, the cp(S-TTCA)/rGO-80 electrode showed an excellent rate performance (shown in Fig. 4d and Fig. S6). For instance, it displayed a highly reversible discharge-charge capacity of 1341 mAh g^{-1} at 0.1 C (shown in Fig. S7) 1220 mAh g^{-1} at 0.2 C, 1017 mAh g^{-1} at 0.5 C, 861 $mAhg^{-1}$ at 1 C, 807 mAh g^{-1} at 2 C, and 645 mAh g^{-1} at 5 C. These rate-capacity values are higher than those of sulfur-embedded benzoxazine polymers [50], covalent triazine frameworks [41], allyl-terminated copolymers, divinylbenzene copolymers [51,52], and the copolymers of S and TTCA supported on carbon black (denoted as cp(S-TTCA)/CB-80 shown in Fig. S8). This was most likely due to the formation of small sulfur-rich polymer crystallites on the highly conductive rGO substrate (Fig. 1). The cycling performance of cp(S-TTCA)/rGO-80 was evaluated at a higher rate current density of 0.5 C. As shown in Fig. 4e, although the specific capacity of cp(S-TTCA)/rGO-80 cathode diminished gradually with prolonging cycling, the discharge voltages remained almost invariant. Fig. 4f shows the cycling performance and coulombic efficiency of the series of cp(S-TTCA)/rGO cathodes. The initial capacity was determined to be 878 mAh g^{-1} for cp(S-TTCA)/rGO-70, 1094 mAh g^{-1} for cp(S-TTCA)/rGO-80 and 1026 $mAhg^{-1}$ for cp(S-TTCA)/rGO-90 at the same sulfur loading of 2 mg cm^{-1}). Yet, after 300 discharge-charge cycles, the specific capacity decreased to 673 mAh g^{-1} for cp(S-TTCA)/rGO-70, 815 mAh g^{-1} for cp(S-TTCA)/rGO-80 and 713 mAh g^{-1} for cp(S-TTCA)/rGO-90, corresponding to a decay rate of 0.088%, 0.098% and 0.121% per cycle, respectively. From these results, one can see that cp(S-TTCA)/rGO-80 stood out as the best among the series.

The long-term cycling stability of the cp(S-TTCA)@rGO-80

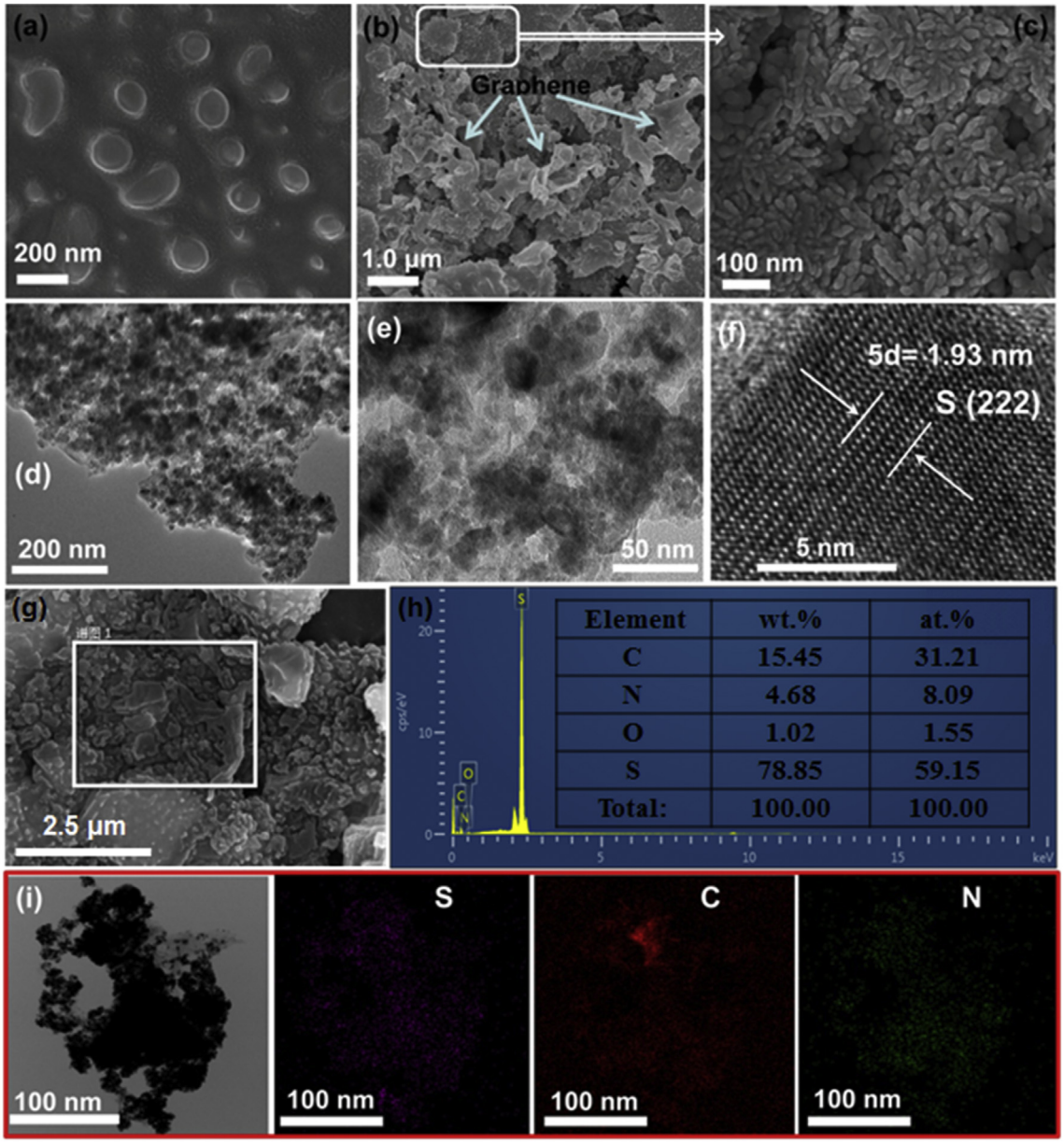

Fig. 3. (a) SEM image of elemental sulfur. (b) SEM image of cp(S-TTCA)@rGO-80 and (c) the corresponding high-resolution SEM image of the selected area in (b). (d, e) TEM images of cp(S-TTCA)@rGO-80 at different magnifications. (f) High-resolution TEM image showing the lattices of crystalline nanoparticles on cp(S-TTCA)@rGO-80. (g) SEM image showing the selected area for EDS measurement; (h) the corresponding EDS spectrum and the summary of element contents. (i) Elemental mapping images of S, C, and N in cp(S-TTCA)@rGO-80. (A colour version of this figure can be viewed online.)

cathode was further studied at a high rate of 1 C. As shown in Fig. 5, after 500 deep charge-discharge cycles, the specific capacity of cp(S-TTCA)@rGO-80 decreased from the initial value of 821 mAh g^{-1} to 671 mAh g^{-1}, corresponding to 81.72% retention and a decay rate of only 0.0404% per cycle. Moreover, the coulombic efficiency was maintained at almost 100%. In contrast, a simple mixture of sulfur and TTCA supported on rGO (denoted as S&TTCA@rGO-80) showed a rapid decrease in capacity, retaining a capacity of ca. 500 mAh g^{-1} after only 300 discharge-charge cycles. The much higher cycling stability of cp(S-TTCA)@rGO-80 is most likely due to the formation of highly crosslinked sulfur copolymers nanoparticles on the rGO surface.

To gain further insights into the structures of cp(S-TTCA)@rGO, we also carried out FTIR measurements (shown in Fig. 6a). The band at 792 cm^{-1} is due to the stretching vibration of the C–S bond [41,53], and the one at 819 cm^{-1} to the stretching vibration of S–S [53]. No apparent change was observed in the FTIR spectrum of cp(S-TTCA)@rGO-80 even after 500 discharge-charge cycles at 1 C, indicating that cp(S-TTCA) is structurally robust. Fig. 6b shows the typical Raman spectra of TTCA@rGO, and cp(S-TTCA)@rGO-80 before and after 500 discharge-charge cycles at 1 C, where one can find that the N=C–S deformation peak in TTCA remains at ca. 439 cm^{-1}, indicating that the thiol groups were still chemically bonded with sulfur. That is, cp(S-TTCA) retained its highly crosslinked networks leading to effective confinement of lithium polysulfides during long-term discharge-charge cycles.

To quantify the crosslinking of sulfur in cp(S-TTCA)@rGO, XPS measurements were conducted (Fig. 7). Calculations based on the integrated peak area of S2s in Fig. 7a suggested that the total S element in the as-synthesized cp(S-TTCA)@rGO-80 was ca. 81.0 wt.%

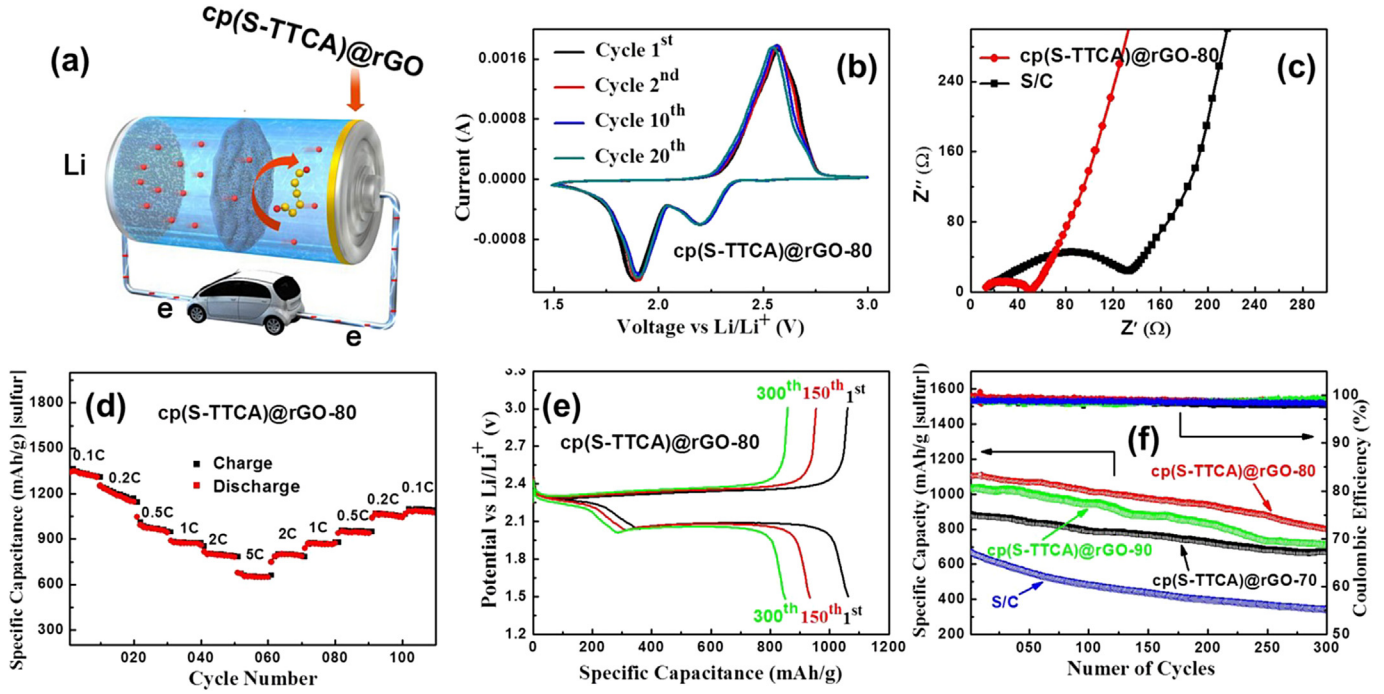

Fig. 4. (a) Schematic illustration of the Li-S battery in the present study. (b) CV curves of the cp(S-TTCA)@rGO-80 cathode at 0.1 mV s^{-1}. (c) EIS curves of cp(S-TTCA)@rGO-80 and S/C cathodes. (d) Rate capacity of the cp(S-TTCA)@rGO-80 cathode at various current densities from 0.1 C to 5 C. (e) The discharge-charge profiles of the cp(S-TTCA)@rGO-80 cathode after various cycles at 0.5 C. (f) Cycling performance and coulombic efficiency of different cathodes at 0.5 C. (A colour version of this figure can be viewed online.)

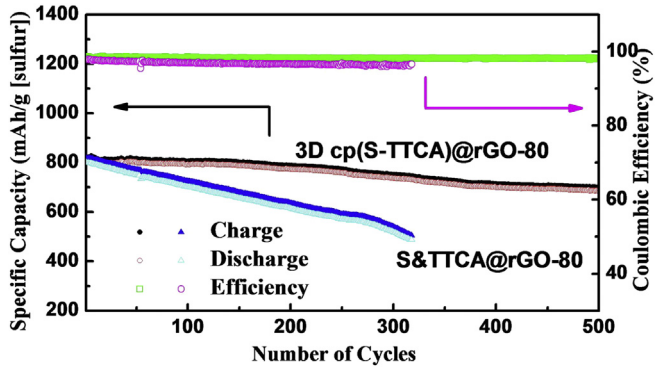

Fig. 5. Long-term cycling performance of cp(S-TTCA)@rGO-80 and S&TTCA@rGO-80 cathodes at 1 C. (A colour version of this figure can be viewed online.)

(red curve). After thoroughly washing with CS_2 to remove the uncrosslinked sulfur (S_8), the total content of S element was determined to be ca. 67.0 wt.% (black curve), which corroborate that about 82.7 wt.% of the feeding sulfur (S_8) has been covalently bonded with TTCA to form crosslinked sulfur-rich polymers in cp(S-TTCA)@rGO-80 composite, which is consistent with the result of TGA measurement in Fig. 2a. Also, on basis of the XPS survey spectra (Fig. 7b–c), the total sulfur content of both cp(S-TTCA)@rGO-80/C and S/C electrodes before and after long-term cycling (500 cycles at 1C for cp(S-TTCA)@rGO-80/C electrode, 300 cycles at 0.5 C for S/C electrode) were determined. As summarized in the histograms in Fig. 7d, the total sulfur content in cp(S-TTCA)@rGO-80/C electrode was 67.5 wt.% before cycling, while it decreased to 49.2 wt.% after cycling, that is about 72.8% of the feeding sulfur (S_8) in synthesis remain bonding with TTCA, corresponding to about 8% loss of the crosslinked sulfur after 500 cycles at 1C. In contrast, the S/C electrode

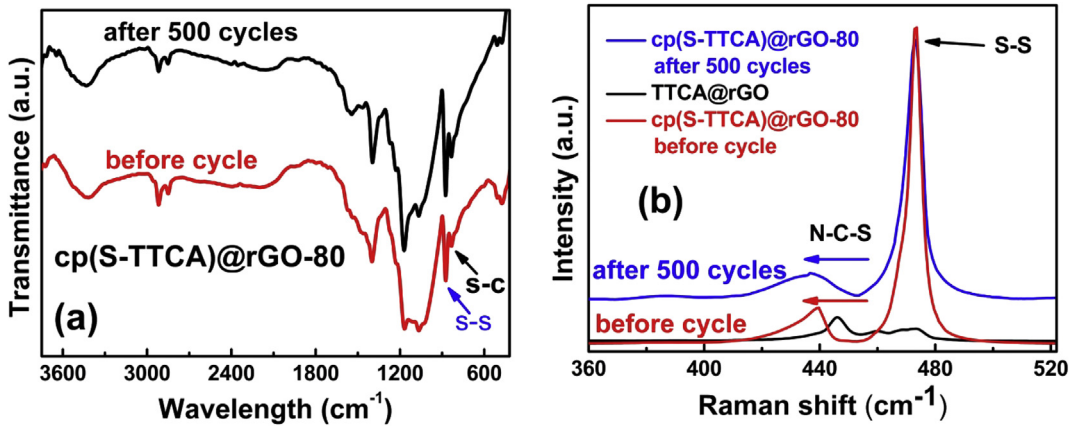

Fig. 6. (a) FTIR spectra of cp(S-TTCA)@rGO before and after 500 discharge-charge cycles at 1C. (b) Raman spectra of pristine TTCA@rGO, and cp (S-TTCA)@rGO before and after 500 discharge-charge cycles at 1C. (A colour version of this figure can be viewed online.)

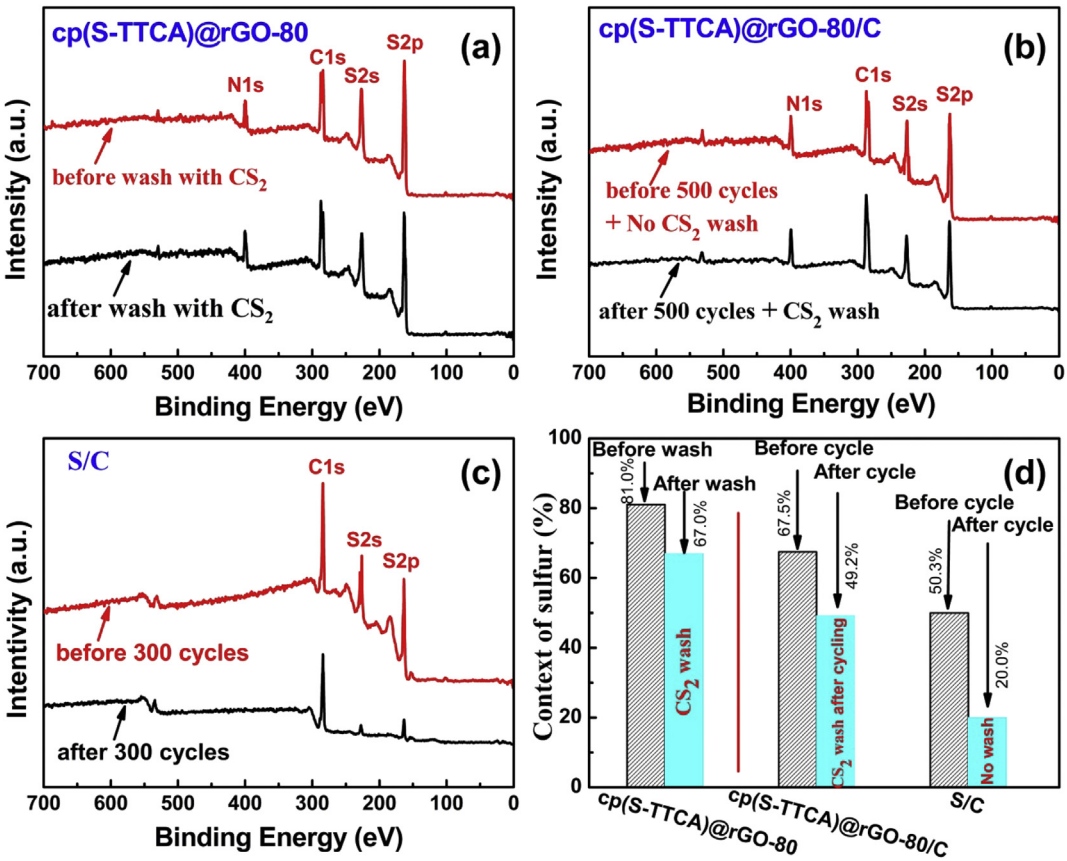

Fig. 7. (a) XPS survey spectra of pristine cp(S-TTCA)@rGO-80 sample before and after washing with CS_2. (b) XPS survey spectra of cp(S-TTCA)@rGO-80/C electrode before discharge-charge cycling and the cp(S-TTCA)@rGO-80/C electrode washed with CS_2 after 500 discharge-charge cycles at 1 C. (c) XPS survey spectra of S/C electrode before discharge-charge cycling and the S/C electrode measured after 500 discharge-charge cycles at 0.5 C without washing with CS_2. (d) Histograms of the sulfur element contents for samples shown in panels a–c. (A colour version of this figure can be viewed online.)

showed a decrease from 50.3 wt.% for the electrode before cycling to 20.0 wt.% for that after cycling, corresponding to ca. 60% loss of sulfur even after only 300 cycles at 0.5 °C. these observations unambiguously show that most of the bonds between sulfur and TTCA are robust to survive after long-term discharge-charge cycling and the significant positive effects of combining both chemical and physical confinements on the performance of Li-S battery.

4. Conclusion

In conclusion, sulfur was copolymerized with TTCA to form highly crosslinked particles on the rGO surface via ring-opening radical polymerization at 170 °C. After polymerization, sulfur was encapsulated into the polymer matrix forming nanoscale crystallites, which helped increase the electrical conductivity and utilization of sulfur. The resulting rate performance was also markedly enhanced with a high discharge capacity of 1341 mAh g^{-1} at 0.1 C and 645 mAh g^{-1} at 5 C. Because of the formation of a large number of chemical bonds between sulfur and TTCA in the cp(S-TTCA)/rGO hybrids, the dissolution and diffusion of polysulfides were substantially reduced, leading to a specific capacity of 671 mAh g^{-1} at 1 C with a retention of 81.72% after 500 deep charge-discharge cycles and a decay rate of only 0.0404% per cycle. These results highlight the significance of chemical confinement of sulfur in enhancing the cathode performance of Li-S batteries, which may be exploited as a fundamental basis for the rational design and engineering of efficient, stable polymer cathodes for high performance Li-S batteries.

Acknowledgements

This work was supported by the National Natural Science Foundation of China (NSFC 21528301 and 51402111), Guangdong Innovative and Entrepreneurial Research Team Program (2014ZT05N200), and the Fundamental Research Funds for the Central Universities (SCUT Grant No. 2153860).

Appendix A. Supplementary data

Supplementary data related to this article can be found at http://dx.doi.org/10.1016/j.carbon.2017.06.036.

References

[1] H.-S. Kang, Y.-K. Sun, Freestanding bilayer carbon-sulfur cathode with function of entrapping polysulfide for high performance Li-S batteries, Adv. Funct. Mater. 26 (8) (2016) 1225–1232.
[2] M.-A. Pope, I.-A. Aksay, Structural design of cathodes for Li-S batteries, Adv. Energy Mater. 5 (2015), 1500124, http://dx.doi.org/10.1002/aenm.201500124.
[3] X. Gu, C.-J. Tong, C. Lai, J. Qiu, X. Huang, W. Yang, et al., A porous nitrogen and phosphorous dual doped graphene blocking layer for high performance Li-S batteries, J. Mater Chem. A 3 (2015) 16670–16678.
[4] W.-J. Chung, J.-J. Griebel, E.-T. Kim, H. Yoon, A.-G. Simmonds, H.-J. Ji, et al., The use of elemental sulfur as an alternative feedstock for polymeric materials, Nat. Chem. 5 (6) (2013) 518–524.
[5] J. Song, M.-L. Gordin, T. Xu, S. Chen, Z. Yu, H. Sohn, et al., Strong lithium polysulfide chemisorption on electroactive sites of nitrogen-doped carbon composites for high-performance lithium-sulfur battery cathodes, Angew. Chem. Int. Ed. 54 (2015) 4325–4329.
[6] H. Wang, W. Zhang, H. Liu, Z. Guo, A strategy for configuration of an integrated flexible sulfur cathode for high-performance lithium-sulfur batteries, Angew.

Chem. Int. Ed. 55 (12) (2016) 3992–3996.
[7] H. Cheng, S. Wang, Recent progress in polymer/sulphur composites as cathodes for rechargeable lithium-sulphur batteries, J. Mater Chem. A 2 (34) (2014) 13783–13794.
[8] L. Borchardt, M. Oschatz, S. Kaskel, Carbon materials for lithium sulfur batteries-ten critical questions, Chem. Eur J. 22 (22) (2016) 7324–7351.
[9] X. Ji, L.-F. Nazar, Advances in Li-S batteries, J. Mater Chem. 20 (2010) 9821–9826.
[10] G.-C. Li, G.-R. Li, S.-H. Ye, X.-P. Gao, A polyaniline-coated sulfur/carbon composite with an enhanced high-rate capability as a cathode material for lithium/sulfur batteries, Adv. Energy Mater. 2 (2012) 1238–1245.
[11] A. Rosenman, E. Markevich, G. Salitra, D. Aurbach, A. Garsuch, F.F. Chesneau, Review on Li-sulfur battery systems: an integral perspective, Adv. Energy Mater. 5 (16) (2015), 1500212, http://dx.doi.org/10.1002/aenm.201500212.
[12] Z. Li, Y. Huang, L. Yuan, Z. Hao, Y. Huang, Status and prospects in sulfur-carbon composites as cathode materials for rechargeable lithium-sulfur batteries, Carbon 92 (92) (2015) 41–63.
[13] G. Li, J. Sun, W. Hou, S. Jiang, Y. Huang, J. Geng, Three-dimensional porous carbon composites containing high sulfur nanoparticle content for high-performance lithium-sulfur batteries, Nat. Commun. 7 (2016) 10601–10608.
[14] M. Yan, Y. Zhang, Y. Li, Y. Huo, Y. Yu, C. Wang, et al., Manganese dioxide nanosheet functionalized sulfur@PEDOT core-shell nanospheres for advanced lithium-sulfur batteries, J. Mater Chem. A 4 (2016) 9403–9412.
[15] B. Li, S. Li, J. Xu, S. Yang, A new configured lithiated silicon-sulfur battery built on 3D graphene with superior electrochemical performances, Energy Environ. Sci. 9 (6) (2016) 2025–2030.
[16] Y. Li, J. Fan, M. Zheng, Q. Dong, A novel synergistic composite, Energy Environ. Sci. 9 (9) (2016) 1998–2004.
[17] S. Rehman, S. Guo, Y. Hou, Rational design of Si/SiO_2 @hierarchical porous carbon spheres as efficient polysulfide reservoirs for high-performance Li-S battery, Adv. Mater. 28 (28) (2016) 3167–3172.
[18] J. Zhang, H. Hu, Z. Li, X.-W. Lou, Double-shelled nanocages with cobalt hydroxide inner shell and layered double hydroxides outer shell as high-efficiency polysulfide mediator for lithium-sulfur batteries, Angew. Chem. Int. Ed. 55 (12) (2016) 3982–3986.
[19] H.-J. Peng, D.-W. Wang, J.-Q. Huang, X.-B. Cheng, Z. Yuan, F. Wei, et al., Janus separator of polypropylene-supported cellular graphene framework for sulfur cathodes with high utilization in lithium-sulfur batteries, Adv. Sci. 3 (1) (2016), 1500268, http://dx.doi.org/10.1002/advs.201500268.
[20] C.-H. Chang, S.-H. Chung, A. Manthiram, Effective stabilization of a high-loading sulfur cathode and a lithium-metal anode in Li-S batteries utilizing SWCNT-modulated separators, Small 12 (2) (2016) 174–179.
[21] Y.-X. Yin, S. Xin, Y.-G. Guo, L.-J. Wan, Lithium-sulfur batteries: electrochemistry, materials, and prospects, Angew. Chem. Int. Ed. 52 (50) (2013) 13186–131200.
[22] Z.-W. Seh, W. Li, J.-J. Cha, G. Zheng, Y. Yang, M.-T. McDowell, et al., Sulphur-TiO_2 yolk-shell nanoarchitecture with internal void space for long-cycle lithium-sulphur batteries, Nat. Commun. 4 (2013) 1331, http://dx.doi.org/10.1038/ncomms2327.
[23] N. Ding, Y. Lum, S. Chen, S.-W. Chien, T.-S.-A. Hor, Z. Liu, et al., Sulfur-carbon yolk-shell particle based 3D interconnected nanostructures as cathodes for rechargeable lithium-sulfur batteries, J. Mater Chem. A 3 (5) (2015) 1853–1857.
[24] L. Qie, A. Manthiram, A facile layer-by-layer approach for high-areal-capacity sulfur cathodes, Adv. Mater. 27 (10) (2015) 1694–1700.
[25] G. Zhou, Y. Zhao, A. Manthiram, Dual-confined flexible sulfur cathodes encapsulated in nitrogen-doped double-shelled hollow carbon spheres and wrapped with graphene for Li-S batteries, Adv. Energy Mater. 5 (9) (2015), http://dx.doi.org/10.1002/aenm.201402263.
[26] J. Kim, D.-J. Lee, H.-G. Jung, Y.-K. Sun, J. Hassoun, B. Scrosati, An advanced lithium-sulfur battery, Adv. Funct. Mater. 23 (8) (2013) 1076–1080.
[27] M. Li, Y. Zhang, X. Wang, W. Ahn, G. Jiang, K. Feng, et al., Gas pickering emulsion templated hollow carbon for high rate performance lithium sulfur batteries, Adv. Funct. Mater. 26 (2016) 8408–8417.
[28] X.-B. Cheng, J.-Q. Huang, Q. Zhang, H.-J. Peng, M.-Q. Zhao, F. Wei, Aligned carbon nanotube/sulfur composite cathodes with high sulfur content for lithium-sulfur batteries, Nano Energy 4 (2014) 65–72.
[29] X. Yang, Y. Yu, N. Yan, H. Zhang, X. Li, H. Zhang, 1-D oriented cross-linking hierarchical porous carbon fibers as a sulfur immobilizer for high performance lithium-sulfur batteries, J. Mater Chem. A 4 (2016) 5965–5972.
[30] J. Song, M.-L. Gordin, T. Xu, S. Chen, Z. Yu, H. Sohn, et al., Strong lithium polysulfide chemisorption on electroactive sites of nitrogen-doped carbon composites for high-performance lithium-sulfur battery cathodes, Angew. Chem. Int. Ed. 54 (14) (2015) 4325–4329.
[31] Z. Li, X. Li, Y. Liao, X. Li, W. Li, Sulfur loaded in micropore-rich carbon aerogel as cathode of lithium-sulfur battery with improved cyclic stability, J. Power Sourc. 334 (2016) 23–30.
[32] J. Ou, L. Yang, Z. Zhang, X. Xi, Honeysuckle-derived hierarchical porous nitrogen, sulfur, dual-doped carbon for ultra-high rate lithium ion battery anodes, J. Power Sourc. 333 (2016) 193–202.
[33] F. Wu, J. Qian, R. Chen, T. Zhao, R. Xu, Y. Ye, et al., Sulfur cathode based on layered carbon matrix for high-performance Li-S batteries, Nano Energy 12 (2015) 742–749.
[34] S. Lu, Y. Cheng, X. Wu, J. Liu, Significantly improved long-cycle stability in high-rate Li-S batteries enabled by coaxial graphene wrapping over sulfur-coated carbon nanofibers, Nano Lett. 13 (6) (2013) 2485–2489.
[35] R. Singhal, S.-H. Chung, A. Manthiram, V. Kalra, A free-standing carbon nanofiber interlayer for high-performance lithium-sulfur batteries, J. Mater Chem. A 3 (2015) 4530–4538.
[36] X. Ji, S. Evers, R. Black, L.-F. Nazar, Stabilizing lithium-sulphur cathodes using polysulphide reservoirs, Nat. Commun. 2 (2011) 325, http://dx.doi.org/10.1038/ncomms1293.
[37] A. Chang, Q. Wu, X. Du, S. Chen, J. Shen, Q. Song, et al., Immobilization of sulfur in microgels for lithium-sulfur battery, Chem. Commun. 52 (2016) 4525–4528.
[38] X. Jia, C. Zhang, J. Liu, W. Lv, D.-W. Wang, Y. Tao, et al., Evolution of the effect of sulfur confinement in graphene-based porous carbons for use in Li-S batteries, Nanoscale 8 (2016) 4447–4451.
[39] S. Diez, A. Hoefling, P. Theato, W. Pauer, Mechanical and electrical properties of sulfur-containing polymeric materials prepared via inverse vulcanization, Polymers 9 (2) (2017) 59–66.
[40] J. Wang, J. Yang, C. Wan, K. Du, J. Xie, N. Xu, Sulfur composite cathode materials for rechargeable lithium batteries, Adv. Funct. Mater. 13 (6) (2003) 487–492.
[41] S.-N. Talapaneni, T.-H. Hwang, S.-H. Je, O. Buyukcakir, J.-W. Choi, A. Coskun, Elemental-sulfur mediated facile synthesis of a covalent triazine framework for high-performance lithium-sulfur batteries, Angew. Chem. 128 (2016) 3158–3163.
[42] B. Li, S. Yang, S. Li, B. Wang, J. Liu, From commercial sponge toward 3D graphene-silicon networks for superior lithium storage, Adv. Energy Mater. 5 (15) (2015), 1500289, http://dx.doi.org/10.1002/aenm.201500289.
[43] H. Kim, J. Lee, H. Ahn, O. Kim, M.-J. Park, Synthesis of three-dimensionally interconnected sulfur-rich polymers for cathode materials of high-rate lithium-sulfur batteries, Nat. Commun. 6 (2015), http://dx.doi.org/10.1038/ncomms8278.
[44] W.-J. Chung, J.-J. Griebel, E.-T. Kim, H. Yoon, A.-G. Simmonds, H.-J. Ji, et al., The use of elemental sulfur as an alternative feedstock for polymeric materials, Nat. Chem. 5 (6) (2013) 518–524.
[45] S. Zeng, L. Li, D. Zhao, J. Liu, W. Niu, N. Wang, et al., Polymer-capped sulfur copolymers as lithium-sulfur battery cathode: enhanced performance by combined contributions of physical and chemical confinements, J. Phys. Chem. C 121 (121) (2017) 2495–2503.
[46] B. Oschmann, J. Park, C. Kim, K. Char, Y.-E. Sung, R. Zentel, Copolymerization of polythiophene and sulfur to improve the electrochemical performance in lithium-sulfur batteries, Chem. Mater. 27 (20) (2015) 7011–7017.
[47] Z. Zhang, H.-K. Jing, S. Liu, G.-R. Li, X.-P. Gao, Encapsulating sulfur into a hybrid porous carbon/CNT substrate as a cathode for lithium-sulfur batteries, J. Mater Chem. A 3 (13) (2015) 6827–6834.
[48] M. Wang, H. Zhang, W. Zhou, X. Yang, X. Li, H. Zhang, Rational design of a nested pore structure sulfur host for fast Li/S batteries with a long cycle life, J. Mater Chem. A 4 (5) (2016) 1653–1662.
[49] S.-A. Abbas, M.-A. Ibrahem, L.-H. Hu, C.-N. Lin, J. Fang, K.-M. Boopathi, et al., Bifunctional separator as a polysulfide mediator for highly stable Li-S batteries, J. Mater Chem. A 4 (24) (2016) 9661–9669.
[50] S.-H. Je, T.-H. Hwang, S.-N. Talapaneni, O. Buyukcakir, H.-J. Kim, J.-S. Yu, et al., Rational sulfur cathode design for lithium-sulfur batteries: sulfur-embedded benzoxazine polymers, ACS Energy Lett. 1 (3) (2016) 566–572.
[51] B.-C. Yu, J.-W. Jung, K. Park, J.-B. Goodenough, A new approach for recycling waste rubber products in Li-S batteries, Energy Environ. Sci. 52 (24) (2016) 4525–4528.
[52] I. Gomez, D. Mecerreyes, J.-A. Blazquez, O. Leonet, H. Ben Youcef, C. Li, et al., Inverse vulcanization of sulfur with divinylbenzene: stable and easy processable cathode material for lithium-sulfur batteries, J. Power Sourc. 329 (2016) 72–78.
[53] W. Li, M. Zhou, H. Li, K. Wang, S. Cheng, K. Jiang, A high performance sulfur-doped disordered carbon anode for sodium ion batteries, Energy Environ. Sci. 8 (10) (2015) 2916–2921.